

# Excited-State Trions in Two Dimensional Materials

Jun Yan

*Department of Physics, University of Massachusetts, Amherst, Massachusetts 01003, USA*

Kalman Varga\*

*Department of Physics and Astronomy, Vanderbilt University, Nashville, Tennessee, 37235, USA*

Using the complex scaling and the stabilization method combined with the stochastic variational approach, we have shown that there are narrow resonance states in two-dimensional three particle systems of electrons and holes interacting via screened Coulomb interaction. These resonances are loosely bound systems of excited state excitons with a third particle circling around them. Recent experimental studies of excited state trions might be explained and identified by these resonant states.

## I. INTRODUCTION

Monolayers of transition metal dichalcogenides (TMD) are chemically and mechanically stable making them ideal systems for studying physics in two dimension (2D). The reduced dimensionality leads to a notably strong Coulomb interaction between charge carriers [1]. This enhanced interaction, in turn, leads to the formation of tightly bound excitons [2–6], charged excitons (trions) [7–11], and biexcitons [12–21].

Theoretical studies [22–39] played an important role in predicting the stability and properties of these electron-hole complexes. Energies of excitons can be calculated by solving the Bethe-Salpeter equation in the quasiparticle band structure framework [25, 26, 40]. The effective mass approach with 2D interaction potential has also been successfully used to calculate binding energies [22, 23, 27–32, 35, 37, 39, 41–43] in good agreement with the BSE approach and the experimental results. In the effective mass models the excitonic systems are considered to be few particle systems, e.g. the trion is bound state of three particles. Other interpretations also exist where trions are described as excitons dressed by interactions with a Fermi sea of excess carriers [38].

Recent experimental studies have shown the existence of excited state trions in TMDs [11, 44]. This is somewhat surprising, because the trion has no known bound excited state. In fact neither the  $H^-$  ( $p, e^-, e^-$ ) nor the  $Ps^-$  ( $e^+, e^-, e^-$ ) ion has bound states in two or three dimensions [45–48]. The  $H^-$  and  $Ps^-$  ion, however, has many resonant states in three dimensions [49–51].

In this paper we will investigate the existence of these resonant states in two dimensional materials. Unlike bound states, the resonances have complex energies and spatially extended non- $L^2$  wave functions. Conventional variational approaches based on square integrable real basis functions can not be directly used to calculate these resonant excited states. We will use two distinct

approaches, the real stabilization method [52], and the complex scaling (CS) [53, 54] approach to find the resonant states. Both of these approaches need a flexible variational basis. We will use the stochastic variational method (SVM) [55] with explicitly correlated Gaussians (ECG) [45] to generate basis states.

The stabilization method (SM) [52] is based on the observation that a sufficiently large-square integrable basis set yields good approximations to the inner part of the exact resonance wave functions at energies equal to the eigenvalues of the Hamiltonian matrix. Eigenvalues belonging to resonant states remain stable when the basis dimension is increased. The degree of stability of the eigenvalues approximating the energy of the resonance is proportional to the width of the resonance. The complex energy of the resonance state can be extracted from the change in the stable eigenvalue as the size of the basis increases.

In the complex scaling method [53, 54], the coordinates are rotated into the complex plane and resonant wave function becomes square-integrable and can be expanded in terms of real basis functions. Trajectory of the eigenenergies of the Hamiltonian as a function of rotation angle are very different for bound, scattering and resonance states. The energy and width of the resonances can be determined from the converged position of the complex eigenvalues.

The stochastic variational method will be used to generate square-integrable basis using explicitly correlated Gaussians [45] for the CS and SM calculations. The SVM has been previously shown to achieve accuracy of up to 8-10 digits when describing the binding energies of similar systems such as  $H_2$ ,  $H_2^+$ , and the positronium molecule ( $Ps_2$ ) [47, 56]. This method has proven to be well-suited for describing the binding energies of excitonic structures ranging from the two-body exciton to five-body exciton-trion systems [30, 46, 48]. Previously, we have shown that this method yields values that agree with other calculations and experimental findings for the binding energies of excitons and trions in TMDs [30, 31].

---

\* kalman.varga@vanderbilt.edu

## II. FORMALISM

### A. Hamiltonian and basis functions

The nonrelativistic Hamiltonian of an excitonic few-particle system is given by

$$H = - \sum_{i=1}^N \frac{\hbar^2}{2m_i} \nabla_i^2 + \sum_{i<j}^N V(r_{ij}), \quad (1)$$

where  $r_{ij} = |\mathbf{r}_i - \mathbf{r}_j|$ , and  $\mathbf{r}_i$ ,  $m_i$ , are the 2D position vector and the effective mass of the particle.

In the case of an excitonic system in 2D, the interaction potential  $V(r_{ij})$  is given by the 2D screened electrostatic interaction potential derived by Keldysh [57]

$$V(r_{ij}) = \frac{q_i q_j}{\kappa r_0} V_{2D} \left( \frac{r_{ij}}{r_0} \right), \quad (2)$$

where

$$V_{2D}(r) = \frac{\pi}{2} [H_0(r) - Y_0(r)]. \quad (3)$$

This potential has been adopted in most of the calculations. Alternative potentials have also been proposed [58] to better describe three atomic sheets that compose a monolayer TMD. In the screened potential  $q_i$  is charge of the  $i$ th particle, and  $r_0$  is the screening length indicative of the medium.  $\kappa$  is the average environmental dielectric constant.  $H_0$  and  $Y_0$  are the Struve function and Bessel function of the second kind, respectively.

The nonlocal macroscopic screening, inherent to 2D systems, distinguishes this potential from its 3D Coulombic counterpart [25]. The length scale of this screening is determined by the 2D layer polarizability  $\chi_{2D}$  as  $r_0 = 2\pi\chi_{2D}/\kappa$ . In the limit of very strong screening ( $r_0 \rightarrow \infty$ ), the potential exhibits a logarithmic divergence, while in the limit of small screening length ( $r_0 \rightarrow 0$ ),  $V(r_{ij})$  approaches the usual  $1/r$  behavior of the Coulomb potential.

The variational method is used to calculate the energy of the system. As a trial function we choose a two dimensional (2D) form of the correlated Gaussians [45, 55]:

$$\exp \left\{ -\frac{1}{2} \sum_{i,j=1}^N A_{ij} \mathbf{r}_i \cdot \mathbf{r}_j \right\}, \quad (4)$$

where  $A_{ij}$  are the nonlinear parameters. The above form of the CG belongs to  $M = 0$ . To allow for  $M \neq 0$  states, we multiply the basis by

$$\prod_{i=1}^N \xi_{m_i}(\mathbf{r}_i), \quad (5)$$

where

$$\xi_m(\boldsymbol{\rho}) = (x + iy)^m. \quad (6)$$

Thus our nonrestrictive CG function reads as

$$\Phi_A(\mathbf{r}) = \mathcal{A} \left\{ \left( \prod_{i=1}^N \xi_{m_i}(\mathbf{r}_i) \right) \times \exp \left\{ -\frac{1}{2} \sum_{i,j=1}^N A_{ij} \mathbf{r}_i \cdot \mathbf{r}_j \right\} \right\}, \quad (7)$$

where  $M = m_1 + m_2 + \dots + m_N$ ,  $m_i$  are integers, and  $\mathcal{A}$  is an antisymmetrizing operator. This function is coupled with the spin function  $\chi_{SM_S}$  to form the trial function. The nonlinear parameters are optimized using the stochastic variational method [45, 55].

Explicitly Correlated Gaussians are very popular in atomic physics and quantum chemistry [45]. The main advantages of ECG bases are: (1) their matrix elements are analytically available for a general N-particle system, (2) they are flexible enough to approximate rapidly changing functions, (3) the permutation symmetry can be easily imposed.

Ref. [45] provides a thorough review of the applications of the ECG basis in various problems. Benchmark tests presented for atoms with  $N=2-5$  electrons show that the ECG basis can produce up to 10 digit accuracy for 2–3 electron atoms. The ECG basis has also proven to be very accurate in calculating weakly bound states. A series of positronic atoms have been predicted using the stochastic variational method with an ECG basis [47, 59]. The binding energy of these systems [45] ranges from 0.001 to 0.04 a.u. (1 a.u. is 27.211 eV) with weakly bound diffuse structures similar to those studied here.

### B. Complex scaling

The complex scaling method was originally proposed by Aguilar, Balslev, and Combes [60, 61]. The CS is introduced by a transformation  $U(\theta)$  with a scaling angle  $\theta$  for the radial coordinate  $\mathbf{r}$

$$U(\theta) \mathbf{r} U^{-1}(\theta) = \mathbf{r} e^{i\theta}, \quad (8)$$

where  $U(\theta)U^{-1}(\theta) = 1$ . The Schrödinger equation,  $H\Psi = E\Psi$ , is transformed as

$$H^\theta \Psi^\theta = E^\theta \Psi^\theta, \quad (9)$$

$$H^\theta = U(\theta) H U^{-1}(\theta), \quad (10)$$

To solve Eq. 10, the wave functions  $\Psi_k^\theta(\mathbf{r})$  are expanded in terms of ECG basis functions:

$$\Psi_k^\theta(\mathbf{r}) = \sum_{i=1}^K c_{ik}(\theta) \Phi_{A_i}(\mathbf{r}), \quad (11)$$

leading to the generalized complex eigenvalue problem

$$\sum_{j=1}^K H_{ij}^\theta c_{jk}(\theta) = E_k^\theta \sum_{j=1}^K O_{ij} c_{jk}(\theta), \quad (12)$$

$$H_{ij}^\theta = \langle \Phi_{A_i} | H^\theta | \Phi_{A_j} \rangle \quad (13)$$

$$O_{ij} = \langle \Phi_{A_i} | \Phi_{A_j} \rangle, \quad (14)$$

where  $H_{ij}^\theta$  are the matrix elements of the complex-scaled Hamiltonian and  $O_{ij}$  is the overlap of the basis functions. In the case of Coulomb interactions the CS Hamiltonian is particularly simple:

$$H_{ij}^\theta = e^{-2\theta} T_{ij} + e^{-\theta} V_{ij} \quad (15)$$

where  $T_{ij}$  and  $V_{ij}$  are the kinetic and potential energy matrices of the ECG basis functions.

The ABC theorem of Aguilar, Combes, and Balslev[60, 61] describes the properties of the of the CS eigenstates:

- (a) Energies of bound states are invariant with respect to the rotation angle.
- (b) Resonance states can be described by square-integrable functions.
- (c) The continuum spectra start at the threshold energies corresponding to the decays of the system into subsystems. The spectra is rotated clockwise by  $2\theta$  from the positive real energy axis.

In the CS method the resonances are determined by finding the position where the complex eigenvalues are stabilized with respect to the rotation angle:

$$\left. \frac{\partial E}{\partial \theta} \right|_{\theta=\theta_{opt}} = \min. \quad (16)$$

Once the position of resonance is determined, the resonance energy ( $E_r$ ) and total width ( $\Gamma$ ) are given by

$$E = E_r - i\frac{1}{2}\Gamma. \quad (17)$$

### C. Stabilization method

In this method we also use a variational ECG basis ansatz

$$\Psi_k^{(K)}(\mathbf{r}) = \sum_{i=1}^K c_{ik} \Phi_{A_i}(\mathbf{r}), \quad (18)$$

but now we use the dimension of the basis,  $K$ , as a parameter (expansion length). The corresponding generalized real eigenvalue problem reads as

$$\sum_{j=1}^K H_{kj}, c_{ji}(\theta) = \epsilon_i^{(K)} \sum_{j=1}^K O_{kj} c_{ji}(\theta), \quad (19)$$

$$H_{ij}^\theta = \langle \Phi_{A_i} | H | \Phi_{A_j} \rangle, \quad (20)$$

$$(21)$$

where  $\epsilon_i^{(K)}$  is the variational estimate to the energy of the  $i$ th state of the system.

The simplest version of the stabilization method [52] is based on the Hylleraas-Undheim theorem [62, 63]. The Hylleraas-Undheim theorem states that (i) comparing

the variational energy estimates obtained with  $K$  trial wavefunctions and the estimate obtained by adding one additional orthonormalized trial wavefunction (increasing the basis dimension to  $K+1$ ), one finds that the new energy estimates are interleaved with the old ones:

$$\epsilon_0^{(K+1)} \leq \epsilon_0^{(K)} \leq \epsilon_1^{(K+1)} \leq \epsilon_1^{(K)} \leq \dots \epsilon_{K-1}^{(K+1)} \leq \epsilon_{K-1}^{(K)} \leq \epsilon_K^{(K+1)} \quad (22)$$

and (ii) the eigenvalues  $\epsilon_i^{(K)}$  are upper limits to the corresponding excited states.

By increasing the basis dimension (“expansion length”) the real part of the resonance energies become “stable”. This stabilization is due to the fact that the inner part of the wave function, at an energy in the resonant region, looks like the wave function of a bound state. The amplitude of the wavefunction in the asymptotic region is much smaller than the amplitude of its inner part. The inner part of the wave function is expanded in a set of discrete exponentially decaying functions, and then the Hamiltonian is diagonalized to yield the approximate resonance energies directly. Once the basis size is sufficiently large to represent the inner part, the energy of this state barely changes when more basis states are added, because the asymptotic part is small and does not contribute to the energy. The energies of the nonresonant scattering wave functions, however, quickly change with the addition of basis states because their asymptotic parts are large.

There are many variants of the stabilization method, one can confine the wave functions with a potential and change the range of confinement, scale the coordinates or perturb the Hamiltonian in some way and find the stable states [64–68]. Most of these approaches can be used to extract the resonance widths as well [64–68].

### D. Stochastic optimization

The basis parameters can be efficiently chosen via the stochastic variational method [55]. In this approach, the variational parameters  $A_{ij}$  of the ECG basis (see Eq. 7) are randomly selected, and the parameters giving the lowest variational energy are retained as basis states. This procedure can be fine-tuned into an efficient optimization scheme as described in detail in Refs. [45, 55].

In the present work we found that the most efficient way to build a flexible basis is as follows:

(i) optimize the ground state on a small ( $K = 200$ ) basis selecting  $A_{ij}$  from a parameter space which confines the interparticle distances below 10 a.u.

(ii) expand the basis by optimizing the lowest  $l$  states by minimizing

$$\sum_{i=1}^l (\epsilon_i^{(K)} - \epsilon)^2 \quad (23)$$

for each  $K$  by SVM. Here  $\epsilon$  can be any number below the lowest eigenvalue. In this step  $A_{ij}$  is chosen allowing

the interparticle distances to extend up to 100 a.u. This helps the description of the extended excited states.

### E. Physical quantities

The following physical quantities will be used to describe the properties of the system and characterize the quality of the wave function. The pair correlation function is defined as

$$C_{pq}(\mathbf{r}) = \frac{2}{N(N-1)} \left\langle \Psi \left| \sum_{i < j}^N \delta(\mathbf{r}_i - \mathbf{r}_j - \mathbf{r}) \right| \Psi \right\rangle, \quad (24)$$

where  $p$  and  $q$  stand for electrons or holes. Using  $C_{pq}(r)$ , the radial part of the correlation function, the powers of inter-particle distances are given by

$$\langle r_{pq}^k \rangle = 2\pi \int_0^\infty r^k C_{pq}(r) r \, dr. \quad (25)$$

### F. Units

The effective electron and hole masses are denoted as

$$m_e^* = m_e m_0 \quad \text{and} \quad m_h^* = m_h m_0 \quad (26)$$

where  $m_0$  is the mass of the electron. One can define an effective Bohr radius as

$$a^* = \frac{\hbar^2 \kappa}{\mu e^2} \quad (27)$$

where  $e$  is the electron's charge and

$$\mu = \frac{m_e^* m_h^*}{m_e^* + m_h^*} \quad (28)$$

is the reduced mass. This can be also written as

$$a^* = \frac{\kappa(1+\sigma)}{m_e} \frac{\hbar^2}{m_0 e^2} = \frac{\kappa(1+\sigma)}{m_e} a_0 \quad \sigma = \frac{m_e}{m_h} \quad (29)$$

where  $a_0 = \frac{\hbar^2}{m_0 e^2}$  is the hydrogenic Bohr radius ( $a_0 = 5.29177 \text{ \AA}$ ). With this one can define

$$\tilde{r}_0 = r_0 / a^*, \quad (30)$$

the screening length normalized by the Bohr radius. Similarly, the effective Bohr energy

$$E^* = \frac{e^2}{\kappa a^*} = \frac{m_e}{\kappa^2(1+\sigma)} E_0, \quad (31)$$

where

$$E_0 = e^2 / a_0 \quad (32)$$

is the Hartree energy ( $E_0 = 27.211 \text{ eV}$ ).

The energy of the exciton and trion states only depends on  $\tilde{r}_0$  and on the electron-hole mass ratio  $\sigma$ . In the following we will use atomic units. The energies of the exciton is analytically known for  $\tilde{r}_0=0$  and  $\sigma = 1$  [69]:

$$E_{ns}^X = -\frac{2}{(2n-1)^2}, \quad (33)$$

that is -2, -2/9 and -2/25 a.u. for the 1s, 2s and the 3s states respectively.

To convert the results to eV and  $\text{\AA}$  one has to multiply the energies by  $E^*$  and the distances by  $a^*$ . This is the same convention as used in Refs. [23, 29, 31]

## III. RESULTS AND DISCUSSION

### A. Spin singlet case

First we present the results for the spin singlet state of the trion. As an illustration of the CS calculation, Fig. 1 shows the lowest 50 eigenvalues as the function of the rotation angle for a trion with  $\sigma = 0$  and  $r_0 = 0$ . The basis dimension in all calculations is  $K = 1500$ . The ground state energy,  $E_0$ , is below the 1s exciton energy ( $E_{1s}^X = -2 \text{ a.u.}$ ), and the resonance state ( $E_1 = -0.28 \text{ a.u.}$ ) below the 2s exciton threshold ( $E_{2s}^X = -2/9 \text{ a.u.}$ ) remains stable. The continuum states rotated to the complex plane with an angle of  $2\theta$ . The first set of continuum states is rotated from the 1s threshold, the second starts at the 2s threshold.

Fig. 2 show the stabilization of the of the energy of trion resonance states. The lowest state,  $E_1 = -0.28 \text{ a.u.}$  (same state is shown on Fig. 1) is stabilized at a small ( $K=200$ ) basis dimension and its energy remains unchanged after that. One can also see that at certain  $K$  values there are “avoided crossings” of the neighboring eigenvalues. The avoided crossing is a simple consequence of the Hylleraas-Undheim theorem. Let's assume that an isolated “stable” eigenvalue  $\epsilon_j^{(K)}$  approximates  $E_1$ . With increasing  $K$  the next higher eigenvalue,  $\epsilon_{j+1}^{(K)}$ , decreases more rapidly than the stable eigenvalue  $\epsilon_j^{(K)}$ , and pushes  $\epsilon_j^{(K)}$  away from  $E_1$ . At this point  $\epsilon_{j+1}^{(K)}$  approaches  $E_1$  and becomes the stable eigenvalue.

The next resonance state,  $E_2$  is slightly below the 2s

threshold and it is also stable from about  $K = 300$ . There

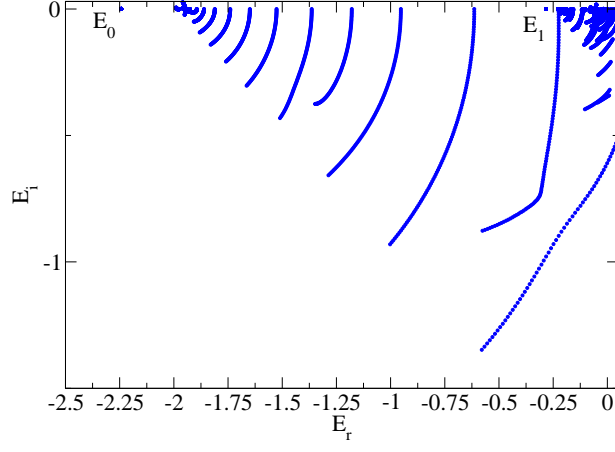


FIG. 1. Trajectories of the complex rotated energies. The energies are rotated from  $\theta = 0$  to  $\theta = 0.36$  (in rad) with a stepsize of  $\Delta\theta = 0.004$  (in rad).  $r_0 = 0$  is used.

$\tilde{r}_0$	$E_r$	$E_i$	$r_{eh}$	$r_{eh}^2$	$\delta_{eh}$	$r_{ee}$	$r_{ee}^2$	$\delta_{ee}$
0	-2.2432	0	0.84	1.20	9.76	1.30	2.28	0.48
	-0.2832	$-8.8 \times 10^{-8}$	4.09	20.93	0.22	7.38	59.98	$9.52 \times 10^{-5}$
	-0.2267	$-1.4 \times 10^{-5}$	9.98	171.58	0.26	18.98	414.41	$2.37 \times 10^{-5}$
	-0.1049	$-1.7 \times 10^{-4}$	12.98	414.39	$6.47 \times 10^{-2}$	24.07	957.33	$1.92 \times 10^{-4}$
	-0.0886	$-1.2 \times 10^{-4}$	16.88	421.15	$3.90 \times 10^{-2}$	32.10	1179.79	$4.52 \times 10^{-4}$
	-0.0814	$-9.3 \times 10^{-5}$	29.82	1463.13	$2.86 \times 10^{-2}$	57.80	3627.17	$8.11 \times 10^{-7}$
0.5	-0.8369	0	1.70	4.72	1.51	2.68	9.32	0.117
	-0.2217	$-3.4 \times 10^{-7}$	5.42	42.86	$7.36 \times 10^{-2}$	9.73	113.38	$1.03 \times 10^{-4}$
	-0.1926	$-5.8 \times 10^{-5}$	29.06	1954.90	$3.76 \times 10^{-2}$	55.01	3911.25	$2.19 \times 10^{-3}$
	-0.0914	$-1.6 \times 10^{-4}$	13.26	287.85	$4.50 \times 10^{-2}$	24.17	720.18	$1.25 \times 10^{-3}$
	-0.0781	$-2.1 \times 10^{-4}$	27.74	1065.93	$1.65 \times 10^{-2}$	43.59	2224.40	$5.70 \times 10^{-5}$
1	-0.5956	0	2.14	7.39	0.90	3.39	14.75	$7.24 \times 10^{-2}$
	-0.1918	$-2.2 \times 10^{-7}$	6.19	51.91	$5.56 \times 10^{-2}$	11.08	138.89	$5.29 \times 10^{-2}$
	-0.1715	$-6.7 \times 10^{-5}$	29.85	1960.28	$5.23 \times 10^{-3}$	56.23	3922.15	$3.84 \times 10^{-2}$
	-0.0841	$-4.2 \times 10^{-4}$	18.16	829.50	$4.34 \times 10^{-2}$	32.73	1809.85	$1.93 \times 10^{-3}$
	-0.0740	$-3.9 \times 10^{-4}$	25.11	1049.68	$5.24 \times 10^{-3}$	45.55	2351.17	$8.46 \times 10^{-5}$

TABLE I. Energies and other properties of trion states for  $S = 0$ . For  $\tilde{r}_0=0$  the ground state and 5 resonance states is shown. For  $\tilde{r}_0 = 0.5$  and  $\tilde{r}_0 = 1$  only four resonance state is listed because the energy of the 5th state is too close to the energy of the  $3s$  exciton and the accurate calculation is very difficult.

are at least two more stable resonant states,  $E_3$  and  $E_4$  below the  $3s$  threshold. Fig. 2 also shows that many states converges to the  $2s$  and  $3s$  thresholds from above. These states represents dissociation into  $2s$  and  $3s$  excitons and an electron.

All these resonance states are stabilized as a straight vertical line which is a typical sign of a narrow resonance. This is conformed by complex scaling as we will see later.

Ref. [50] also found 4 resonant states in the three dimensional case. The energies are obviously different in 2D and 3D, but there are two resonances below the  $2s$  threshold in both 2D and 3D. Ref. [50] shows two resonances below the  $3s$  threshold, our complex scaling approach shows at least 3 states.

By enlarging the CS calculation results in Fig. 1

around the resonant states, Fig. 3 shows 4 narrow resonance states in the complex energy plane. This is the same 4 states that is calculated by the stabilization method and shown in Fig. 2. These are all very narrow resonances.

Fig. 4 shows the electron-electron and the electron hole correlation functions for the ground state of trion. Due to the presence of the second electron the electron-hole correlation function is somewhat wider than that of the exciton. The electron-electron correlation function is pushed away from the origin due to the repulsion. The structure of the trion is more or less similar to a system where an electron is orbiting around an exciton.

The exciton plus electron structure of the excited states show very similar tendency. Fig. 5 shows the



correlation functions for the 4 resonance states.  $E_1$  and  $E_2$  are below the  $2s$  exciton threshold and they have a pronounced  $2s$  exciton plus an outer electron structure. The electron-hole correlation function of the excited state trion is very similar to the electron-hole density in the exciton. The difference between the excited trion with energy  $E_1$  and  $E_2$  is that in the latter the second electron is much farther away from the exciton (as the electron-electron correlation function shows in Fig. 5). In the trion with energy  $E_2$  the electron-hole correlation has a long tail overlapping with the electron electron-correlation function. The second electron strongly polarizes the exciton. The excited trion binding is due to the significant overlap between the electron-electron and electron-hole correlation functions. The excited states with energy  $E_3$  and  $E_4$  show very similar tendency, an  $3s$  exciton plus an electron far out from the center.

The energies and the average distances between particles are compared in Table I for different  $\tilde{r}_0$  values. Compared to the compact ground state trions, the electron-hole and electron-electron distances are very large in the excited states. The large size is explained by the facts that the excited exciton is larger and the are loosely bound states are more extended. Table I. also shows

$$\delta_{ee} = C_{ee}(0), \quad \text{and} \quad \delta_{eh} = C_{eh}(0) \quad (34)$$

the probability that the two electron or an electron and the hole are at the same spatial position. This probability is decreasing with the increased spatial distribution and the probability for electron-hole is always larger than that of the electron-electron.

To calculate resonance states for  $0 < \tilde{r}_0$  we use the ECG basis that is generated by SVM for  $\tilde{r} = 0$ . The basis dimension is very large ( $K = 1500$ ) and the basis is flexible enough to be accurate for nonzero  $\tilde{r}_0$ . Actually the  $\tilde{r}_0 = 0$  case is the most challenging calculation because of the deep Coulomb potential near the origin. Increasing  $\tilde{r}_0$  leads to less attractive potential close to the origin, while the asymptotic part ( $r > 5$ ) of the potential still behaves like  $1/r$ . This asymptotic Coulomb part determines the resonance wave functions beyond  $r = 5$  so one expects that the resonances also exist for  $0 < \tilde{r}_0$ .

Using the ECG basis optimized for  $\tilde{r}_0 = 0$  we show the change of the calculated resonance energies as a function  $\tilde{r}_0$  in Fig. 6. We have optimized the ECG basis for several  $\tilde{r}_0$  values and used CS to check that the resonance energy trajectory in Fig. 6 is accurate.

The calculated total energies and the binding energies for the ground state and the lowest two resonance states are shown in Figs. 7 and 8. We only show these two resonance states because the energy of the higher states barely depends on  $\tilde{r}_0$  (see. Table I.). This is not surpris-

ing, the resonance states with higher energy only feel the  $1/r$  tail of the potential which is independent of  $\tilde{r}_0$ . The weak  $\tilde{r}_0$  dependence is also true for the resonances with energy  $E_1$  and  $E_2$  above  $\tilde{r}_0 = 1$ . The mean distances between particles at  $\tilde{r}_0 = 1$  are larger than  $r = 5$  (see Table I.) so these states are mostly affected by the Coulomb tail. Energies  $E_1$  and  $E_2$  proportional to the energy of the  $2s$  trion (see Fig. 7) and the binding energy hardly changes (see Fig. 8).

The most interesting feature of the dependence of the binding energies on  $\tilde{r}_0$  is that the excited states become more bound than the ground state by increasing  $\tilde{r}_0$ . The trajectory of  $E_1$  and  $E_0$  crosses at  $\tilde{r}_0 = 0.55$  and  $E_2$  and  $E_0$  crosses at  $\tilde{r}_0 = 1.4$ . This happens because the ground state wave function (see Fig. 4) is nonzero close to the origin and increasing  $\tilde{r}_0$  weakens the potential in that region and the ground state binding energy rapidly decreases with  $r_0$  as Fig. 8 shows. As it was already mentioned, the excited states are mostly governed by the Coulomb tail and their energies are less sensitive to  $\tilde{r}_0$ .

The correlation functions of the excited states for  $\tilde{r}_0 > 0$  is very similar to the  $\tilde{r} = 0$  case shown in Fig. 5, but spatially more extended. This is because increasing  $\tilde{r}_0$  the total energies are decreasing and the size of the states are increasing (see Table I.). As an illustration of the similarity we show the ground state trion for  $\tilde{r}_0 = 0$  and  $\tilde{r}_0 = 1$  in Fig. 4.

We have also investigated the effect of electron and hole mass ratio on the binding energy. By using different masses the electron hole the electron hole symmetry is broken so we have two different trions,  $ehh$  and  $eeh$ . To magnify the binding energy differences, we have used a relatively large hole mass by choosing  $\sigma = 2/3$ . For smaller hole masses the tendencies in the binding energies can not be easily illustrated. Fig. 9 shows the binding energy of  $ehh$  and  $eeh$  as a function of  $\tilde{r}_0$ . The heavier hole leads to larger binding energies compared to the  $\sigma = 1$  case, and the  $ehh$  system is has larger binding energy than  $eeh$ , except for the  $E_2$  resonance where the two energies are nearly equal. The mass difference also affects the crossing points.

## B. Spin triplet case

Similarly to the 3D case [50], we have also found two resonances for spin triplet trions in 2D, one right below the  $2s$  threshold and one very close to the  $3s$  threshold, so the binding energies of these resonances is very small (see Table II.). The average distances in these systems are very similar to the those of the singlet  $E_1$  and  $E_3$ , respectively.

---

Fig. 10 compares the correlation function of the exciton and the triplet trion resonances. Once again, the

---

electron-hole correlation function is very similar to the  $2s$  and  $3s$  exciton. The peak of electron-electron correla-

$E_r$	$E_i$	$r_{eh}$	$r_{eh}^2$	$\delta_{eh}$	$r_{ee}$	$r_{ee}^2$	$\delta_{ee}$
-0.2254	$-5.0 \times 10^{-6}$	11.94	256.66	0.16	22.88	599.55	$1.5 \times 10^{-12}$
-0.0845	$-1.2 \times 10^{-6}$	19.61	573.79	0.03	37.72	1568.04	$1.9 \times 10^{-11}$

TABLE II. Energies and other properties of trion states for  $S = 1$ ,  $\tilde{r}_0=0$  and  $\sigma = 1$ .

tion function, however, is almost twice as far away then in the singlet case (see Fig. 5  $E_1$  and  $E_3$ ) because the two electron has parallel spins.

### C. Comparison to experiments

In this section we compare the calculated results to experimental measurements in monolayer TMDs sandwiched between hexagonal boron nitride. The encapsulation of TMD monolayers between atomically smooth hexagonal boron nitride layers allow high quality optical measurements. Binding energies and radii of Rydberg exciton states and energies of charged excitons were measured in  $\text{WS}_2$  [2, 11],  $\text{WSe}_2$  [5, 19, 43, 70–72],  $\text{MoS}_2$  [1, 7, 73–76],  $\text{MoSe}_2$  [74, 77] and  $\text{MoTe}_2$  [74, 77].

Using the parameters ( $\mu$ ,  $r_0$ , and  $\kappa$ ) given in Table I. of Ref. [74] we have calculated the binding energies and root mean square distances of excitons and trions in  $\text{WS}_2$ ,  $\text{WSe}_2$ ,  $\text{MoSe}_2$ ,  $\text{MoS}_2$  and  $\text{MoTe}_2$  (Table III.). Note, that in some cases the  $\tilde{r}_0$  values are very different, but the energies are very similar. For example, the binding energies of  $\text{WS}_2$  and  $\text{WSe}_2$  are very close despite of the difference in  $\tilde{r}_0$ . This is because the change of binding energy between  $\tilde{r}_0=0.59$  and  $\tilde{r}_0=0.84$  is compensated by the slightly larger  $E^*$  of  $\text{WSe}_2$ .  $E^*$  is inversely proportional to  $\kappa^2$  so small changes in  $\kappa$  can cause large energy changes.

The calculated binding energies and radii for excitons (Table III.) are in excellent agreement with the experimental binding energy and radii of Table I of [74], reproducing the fit of the model to experimental data of Ref. [74]. The calculated exciton radii and energies are also in agreement with the calculated and the experimental values for  $\text{WSe}_2$  [6] (the calculated  $r_{eh}^2=1.67$  nm for  $1s$  and  $r_{eh}^2=6.96$  nm for  $2s$ , the experimental values are 1.7 nm and 6.6 nm, the calculated  $E_{2s} - E_{1s}$  is 124 meV, the experimental value is 130 meV).

In previous calculations (see Table II. of Ref. [31]) for TMDs suspended in vacuum or placed on  $\text{SiO}_2$  substrate the calculated and experimental energies of excitons were 50-100 meV different. The new and more accurate measurements using monolayer TMDs sandwiched between hexagonal boron nitrades allow the study of the Rydberg states of excitons in magnetic field and one can extract the binding energy and radii of the Rydberg states [74]. These physical properties then can be used to find the most suitable model parameters, reducing the difference between the experimental and theoretical binding energy of excitons to less than 5 meV.

The agreement of calculated and experimental binding

energies (Table III.) are not as good as for excitons, but in general it is similar to the agreement for the TMDs suspended in vacuum or placed on  $\text{SiO}_2$  surface [31, 35]. Comparing the experimental and calculated trion energies one has to keep in mind that the model parameters were fitted to the exciton measurements [74], but the trion energies was measured in the same experiment. For example, the  $E_{2s} - E_{1s}$  energy difference was measured to be 141.7 meV for  $\text{WS}_2$  in Ref. [74]. The value of this transition energy is very important to find the screening length. In Ref. [11] trion states at 31 and 37 meV were reported in  $\text{WS}_2$ , but the  $E_{2s} - E_{1s}$  difference was measured to be 145 meV in the this experiment. This small difference (141.7 meV to fit the parameter and 145 meV in the measurement) would lead to relatively large change in the model parameters and would affect the binding energy of the trions. Another factor to consider is the effective mass,  $\mu$ . The energy of the exciton only depends on  $\mu$  so the experiments can only pinpoint the reduced mass but give no guidance about effective mass of the hole. In the calculations presented in Table III. we used  $m_e = m_h$  ( $\sigma = 1$ ). As it is illustrated in Fig. 9, using different values for the electron and hole mass while keeping the reduced mass the same increases the binding energies. For the energy of trions in TMDs (see Table III.) this would lead to a 3-5 meV increase in binding energies.

The calculated binding energy for the excited-state trions is about the same range as the ground state binding energies, these excited states have relatively large binding energies. Excited-state trion was recently reported in  $\text{WS}_2$  [11] and  $\text{MoSe}_2$  [44] with binding energies close to the binding energy of the ground state. The width of these resonance states are very small and these are quasi-bound states. In the lower excited state,  $E_1$ , the  $eh$  and  $ee$  distances about 2.5 to 3 times larger than in the ground state. This state is an  $2s$  exciton with an loosely bound electron (or hole) circling around it. The second excited state,  $E_2$ , is even larger with tens of nanometers of distances between  $ee$  and  $eh$ . Due the large size this state is a model prediction in a perfect 2D system, but it is unlikely that this can be measured in a real material.

Fig. 8 can be used as a guide to analyze the agreement between the Keldysh potential based models and experiments. If the energy differences between the Rydberg exciton states are measured, one can choose the most suitable  $\tilde{r}_0$  value using the top part of Fig. 8. This value then can be used to predict the trion energies using the bottom part of Fig. 8.

#### IV. SUMMARY

Using the complex scaling and the stabilization method combined with the stochastic variational approach, we have studied resonance states of three-particle systems interacting with a Coulomb and a screened Coulomb (Keldysh potential). The stochastic variational method was used to generate a suitable square integrable basis of explicitly correlated Gaussians. The stochastic variational method has been previously used [31, 35] to describe trions, biexcitons and charged biexcitons in TMDs and in high precision calculations in atomic and molecular systems [45]. We have used two independent approaches, the complex scaling and the stabilization to calculate the resonance states using real basis functions.

In 2D Coulomb three particles systems with  $S = 0$ , we have found three resonance states below the  $2s$  and two resonance states below the  $3s$  two-particle (exciton) threshold. These states can be envisioned as a  $2s$  or  $3s$  exciton with a third, loosely bound particle circling around it. Comparing the correlation functions of  $2s$  and  $3s$  excitons to those of the excited trions confirm that picture. We have also found 2 resonance states for  $S = 1$ . Resonance states similar to these have been studied in 3D for Coulomb potential [50]. These resonances are mostly due to the long tail of the Coulomb interaction and they

survive the confinement from 3D to 2D, despite of the fact that their energy and spatial extension radically changes.

Screening the Coulomb interaction using a Keldysh potential changes the energy of these resonances, but they remain narrow quasi-bound states. The screening decreases the Coulomb potential at the origin, pushing the resonance wave function farther out, so the interparticle distances quickly increases. As the wave functions of the resonance states are mostly feel the Coulomb tail, the resonance energies are less sensitive to the screening than the energy of the ground state. At some screening length the binding energy of the resonance states will be larger than that of the ground state.

We have calculated the energies and interparticle distances of these resonance states for various TMDs. Energies of excited-state trions in  $\text{WS}_2$  [11] and  $\text{MoSe}_2$  [44] are reasonably close to the values predicted by the calculations. Closer agreement may require more elaborate calculations including spin-orbit interactions and multi-band Hamiltonians as used, for example, in Ref. [35].

#### ACKNOWLEDGMENTS

K.V. was supported by the National Science Foundation (NSF) under Grant No. IRES 1826917, J.Y. acknowledges support by NSF ECCS-1509599.

- 
- [1] K. F. Mak, C. Lee, J. Hone, J. Shan, and T. F. Heinz, *Phys. Rev. Lett.* **105**, 136805 (2010).
  - [2] A. Chernikov, T. C. Berkelbach, H. M. Hill, A. Rigosi, Y. Li, O. B. Aslan, D. R. Reichman, M. S. Hybertsen, and T. F. Heinz, *Phys. Rev. Lett.* **113**, 076802 (2014).
  - [3] M. M. Ugeda, A. J. Bradley, S.-F. Shi, F. H. da Jornada, Y. Zhang, D. Y. Qiu, W. Ruan, S.-K. Mo, Z. Hussain, Z.-X. Shen, F. Wang, S. G. Louie, and M. F. Crommie, *Nat. Mater.* **13**, 1091 (2014).
  - [4] Ye Ziliang, Cao Ting, O'Brien Kevin, Zhu Hanyu, Yin Xiaobo, Wang Yuan, Louie Steven G., and Zhang Xiang, *Nature* **513**, 214218 (2014).
  - [5] K. He, N. Kumar, L. Zhao, Z. Wang, K. F. Mak, H. Zhao, and J. Shan, *Phys. Rev. Lett.* **113**, 026803 (2014).
  - [6] A. V. Stier, N. P. Wilson, K. A. Velizhanin, J. Kono, X. Xu, and S. A. Crooker, *Phys. Rev. Lett.* **120**, 057405 (2018).
  - [7] K. F. Mak, K. He, C. Lee, G. H. Lee, J. Hone, T. F. Heinz, and J. Shan, *Nat. Mater.* **12**, 207 (2013).
  - [8] B. Zhu, H. Zeng, J. Dai, Z. Gong, and X. Cui, *Proc. Natl. Acad. Sci. U.S.A.* **111**, 11606 (2014).
  - [9] G. Wang, L. Bouet, D. Lagarde, M. Vidal, A. Balocchi, T. Amand, X. Marie, and B. Urbaszek, *Phys. Rev. B* **90**, 075413 (2014).
  - [10] C. Zhang, H. Wang, W. Chan, C. Manolatou, and F. Rana, *Phys. Rev. B* **89**, 205436 (2014).
  - [11] A. Arora, T. Deilmann, T. Reichenauer, J. Kern, S. Michaelis de Vasconcellos, M. Rohlfing, and R. Bratschkitsch, *Phys. Rev. Lett.* **123**, 167401 (2019).
  - [12] Y. You, X.-X. Zhang, T. C. Berkelbach, M. S. Hybertsen, D. R. Reichman, and T. F. Heinz, *Nat. Phys.* **11**, 477 (2015).
  - [13] G. Plechinger, P. Nagler, J. Kraus, N. Paradiso, C. Strunk, C. Schiller, and T. Korn, *Phys. Status Solidi RRL* **9**, 457 (2015).
  - [14] Y. Meng, T. Wang, Z. Li, Y. Qin, Z. Lian, Y. Chen, M. C. Lucking, K. Beach, T. Taniguchi, K. Watanabe, S. Tongay, F. Song, H. Terrones, and S.-F. Shi, *Nano Letters* **19**, 299 (2019).
  - [15] C. E. Stevens, J. Paul, T. Cox, P. K. Sahoo, H. R. Gutiérrez, V. Turkowski, D. Semenov, S. A. McGill, M. D. Kapetanakis, I. E. Perakis, D. J. Hilton, and D. Karaickaj, *Nature Communications* **9**, 3720 (2018).
  - [16] M. Barbone, A. R. P. Montblanch, D. M. Kara, C. Palacios-Berraquero, A. R. Cadore, D. De Fazio, B. Pingault, E. Mostaani, H. Li, B. Chen, K. Watanabe, T. Taniguchi, S. Tongay, G. Wang, A. C. Ferrari, and M. Atatüre, *Nature Communications* **9**, 3721 (2018).
  - [17] S.-Y. Chen, T. Goldstein, T. Taniguchi, K. Watanabe, and J. Yan, *Nature Communications* **9**, 3717 (2018).
  - [18] Z. Li, T. Wang, Z. Lu, C. Jin, Y. Chen, Y. Meng, Z. Lian, T. Taniguchi, K. Watanabe, S. Zhang, D. Smirnov, and



system	property	method	WS <sub>2</sub>	WSe <sub>2</sub>	MoS <sub>2</sub>	MoSe <sub>2</sub>	MoTe <sub>2</sub>
	$\tilde{r}_0$		0.5942	0.8399	0.8923	1.3324	2.2489
<i>eh</i>	$E_{1s}$	calc	-178.7	-161.4	-220.2	-231.9	-176.9
	$E_{1s}$	exp	-180 <sup>a</sup>	-167 <sup>a</sup> , -170 <sup>h</sup>	-221 <sup>a,i</sup>	-231 <sup>a</sup>	-177 <sup>a</sup>
	$\sqrt{\langle r_{eh}^2 \rangle}$	calc	1.66	1.68	1.23	1.10	1.31
	$\sqrt{\langle r_{eh}^2 \rangle}$	exp	1.8 <sup>a</sup>	1.7 <sup>a,b</sup>	1.2 <sup>a</sup>	1.1 <sup>a</sup>	1.3 <sup>a</sup>
	$E_{2s}$	calc	-37.8	-37.4	-51.8	-60.6	-52.8
	$\sqrt{\langle r_{eh}^2 \rangle}$	calc	7.20	6.97	5.08	4.32	4.81
	$\sqrt{\langle r_{eh}^2 \rangle}$	exp		6.6 <sup>b</sup>			
	$E_{2s} - E_{1s}$	calc	140.9	124	168.4	171.3	124.1
	$E_{2s} - E_{1s}$	exp	141.7 <sup>a</sup>	130 <sup>b</sup> , 131 <sup>h</sup>	170 <sup>a,i</sup>	168 <sup>a</sup> , 148 <sup>j</sup> , 152 <sup>c</sup>	124 <sup>a,j</sup>
<i>eeh</i>	$E_0$	calc	-194.4	-175.2	-238.8	-250.8	-190.5
	$E_0^b$	calc	15.7	13.8	16.6	18.9	13.6
	$E_0^b$	exp	27, 31 <sup>d</sup>	21, 29 <sup>e</sup>	17, 25 <sup>f</sup>	27 <sup>c,g</sup>	
	$\sqrt{\langle r_{eh}^2 \rangle}$	calc	3.01	3.05	2.2	2.0	2.4
	$\sqrt{\langle r_{ee}^2 \rangle}$	calc	4.24	4.03	3.2	2.8	3.4
	$E_1$	calc	-54.1	-53.8	-74.4	-87.3	-75.5
	$E_1^b$	calc	16.3	16.4	22.6	26.6	22.7
	$E_1^b$	exp	22 <sup>d</sup>			27 <sup>c</sup>	
	$\sqrt{\langle r_{eh}^2 \rangle}$	calc	8.5	8.83	6.1	5.5	5.8
	$\sqrt{\langle r_{ee}^2 \rangle}$	calc	13.9	14.20	9.9	8.8	9.4
	$E_2$	calc	-48.0	-48.1	-66.8	-78.8	-67.9
	$E_2^b$	calc	10.2	10.7	15.1	18.2	15.1
	$\sqrt{\langle r_{eh}^2 \rangle}$	calc	54.9	45.8	29.0	28.2	29.3
	$\sqrt{\langle r_{ee}^2 \rangle}$	calc	77.6	64.9	41.1	40.0	41.4

TABLE III. Energies and mean distances in TMDs. Energies are in meV, distances and in nm,  $E_1^b = E_1 - E_{1s}$ ,  $E_2^b = E_2 - E_{2s}$ ,  $E_3^b = E_3 - E_{2s}$ . The experimental values are taken from: <sup>a</sup> [74], <sup>b</sup> [6], <sup>c</sup> [44], <sup>d</sup> [11], <sup>e</sup> [17], <sup>f</sup> [73], <sup>g</sup> [71] <sup>h</sup> [78], <sup>i</sup> [76], <sup>j</sup> [77]

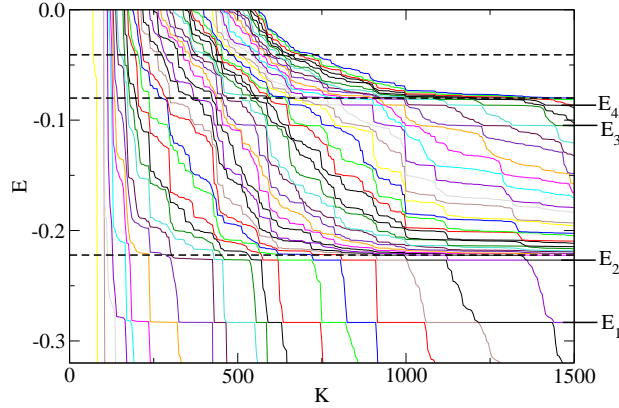


FIG. 2. Energy levels versus basis dimension. The four excited states energies ( $E_1, E_2, E_3$  and  $E_4$ ) are nicely stabilized as the energies are converging with the increased basis size.  $\tilde{r}_0=0$  is used. The dashed lines show the  $2s$ ,  $3s$  and  $4s$  exciton energies.

- S.-F. Shi, Nature Communications **9**, 3719 (2018).
- [19] Z. Ye, L. Waldecker, E. Y. Ma, D. Rhodes, A. Antony, B. Kim, X.-X. Zhang, M. Deng, Y. Jiang, Z. Lu, D. Smirnov, K. Watanabe, T. Taniguchi, J. Hone, and T. F. Heinz, Nature Communications **9**, 3718 (2018).
- [20] M. He, P. Rivera, D. Van Tuan, N. P. Wilson, M. Yang, T. Taniguchi, K. Watanabe, J. Yan, D. G. Mandrus, H. Yu, H. Dery, W. Yao, and X. Xu, Nature Communications **11**, 618 (2020).
- [21] W. Wang, N. Sui, M. Ni, X. Chi, L. Pan, H. Zhang, Z. Kang, Q. Zhou, and Y. Wang, The Journal of Physical Chemistry C **124**, 1749 (2020).
- [22] I. Kylänpää and H.-P. Komsa, Phys. Rev. B **92**, 205418 (2015).
- [23] T. C. Berkelbach, M. S. Hybertsen, and D. R. Reichman, Phys. Rev. B **88**, 045318 (2013).

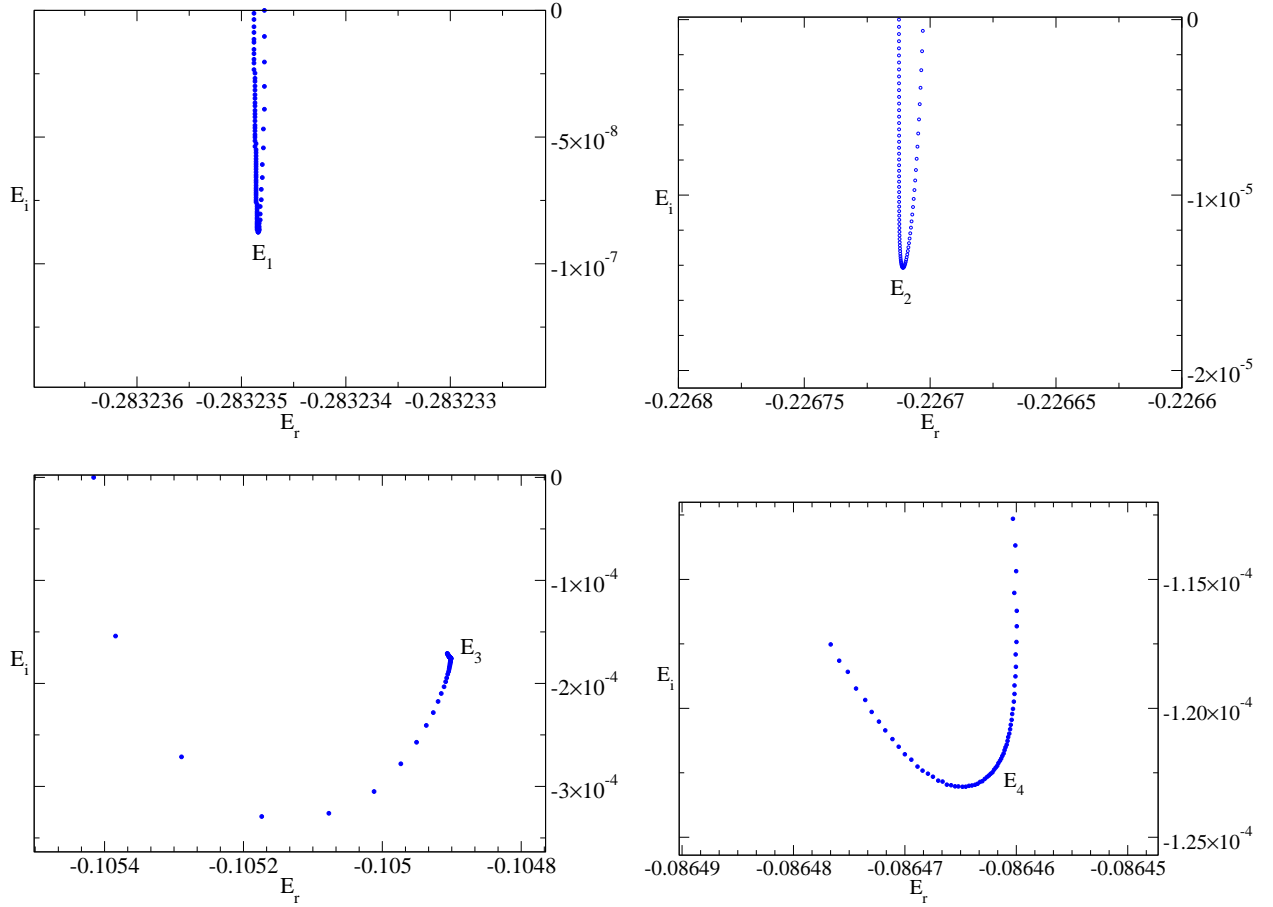


FIG. 3. Trajectories of the excited states of trion on the complex energy plane. The energies are rotated from  $\theta = 0$  to  $\theta = 0.1$  with a stepsize of  $\Delta\theta = 0.004$  (in rad).  $\tilde{r}_0 = 0$  is used.

- [24] G. Berghäuser and E. Malic, Phys. Rev. B **89**, 125309 (2014).
- [25] P. Cudazzo, I. V. Tokatly, and A. Rubio, Phys. Rev. B **84**, 085406 (2011).
- [26] M. Bieniek, L. Szulakowska, and P. Hawrylak, Phys. Rev. B **101**, 125423 (2020).
- [27] B. Ganchev, N. Drummond, I. Aleiner, and V. Fal'ko, Phys. Rev. Lett. **114**, 107401 (2015).
- [28] M. Z. Mayers, T. C. Berkelbach, M. S. Hybertsen, and D. R. Reichman, Phys. Rev. B **92**, 161404 (2015).
- [29] K. A. Velizhanin and A. Saxena, Phys. Rev. B **92**, 195305 (2015).
- [30] D. K. Zhang, D. W. Kidd, and K. Varga, Nano Letters **15**, 7002 (2015).
- [31] D. W. Kidd, D. K. Zhang, and K. Varga, Phys. Rev. B **93**, 125423 (2016).
- [32] E. Prada, J. V. Alvarez, K. L. Narasimha-Acharya, F. J. Bailen, and J. J. Palacios, Phys. Rev. B **91**, 245421 (2015).
- [33] S. C. Kuhn and M. Richter, Phys. Rev. B **101**, 075302 (2020).
- [34] S. C. Kuhn and M. Richter, Phys. Rev. B **99**, 241301 (2019).
- [35] M. Van der Donck, M. Zarenia, and F. M. Peeters, Phys. Rev. B **96**, 035131 (2017).
- [36] D. Van Tuan, B. Scharf, Z. Wang, J. Shan, K. F. Mak, I. Žutić, and H. Dery, Phys. Rev. B **99**, 085301 (2019).
- [37] E. Mostaani, M. Szyniszewski, C. H. Price, R. Maezono, M. Danovich, R. J. Hunt, N. D. Drummond, and V. I. Fal'ko, Phys. Rev. B **96**, 075431 (2017).
- [38] D. K. Efimkin and A. H. MacDonald, Phys. Rev. B **95**, 035417 (2017).
- [39] S. Wu, L. Cheng, and Q. Wang, Phys. Rev. B **100**, 115430 (2019).
- [40] T. Deilmann and K. S. Thygesen, Phys. Rev. B **96**, 201113 (2017).
- [41] R. Y. Kezerashvili, Few-Body Systems **60**, 52 (2019).
- [42] M. Van der Donck, M. Zarenia, and F. M. Peeters, Phys. Rev. B **97**, 195408 (2018).
- [43] E. Courtade, M. Semina, M. Manca, M. M. Glazov, C. Robert, F. Cadiz, G. Wang, T. Taniguchi, K. Watanabe, M. Pierre, W. Escoffier, E. L. Ivchenko, P. Renucci, X. Marie, T. Amand, and B. Urbaszek, Phys. Rev. B **96**, 085302 (2017).
- [44] J. Y. et. al., .
- [45] J. Mitroy, S. Bubin, W. Horiuchi, Y. Suzuki, L. Adamowicz, W. Cencek, K. Szalewicz, J. Komasa, D. Blume, and K. Varga, Rev. Mod. Phys. **85**, 693 (2013).
- [46] J. Usukura, Y. Suzuki, and K. Varga, Phys. Rev. B **59**, 5652 (1999).
- [47] K. Varga, Phys. Rev. Lett. **83**, 5471 (1999).
- [48] C. Riva, F. M. Peeters, and K. Varga, Phys. Rev. B **61**,

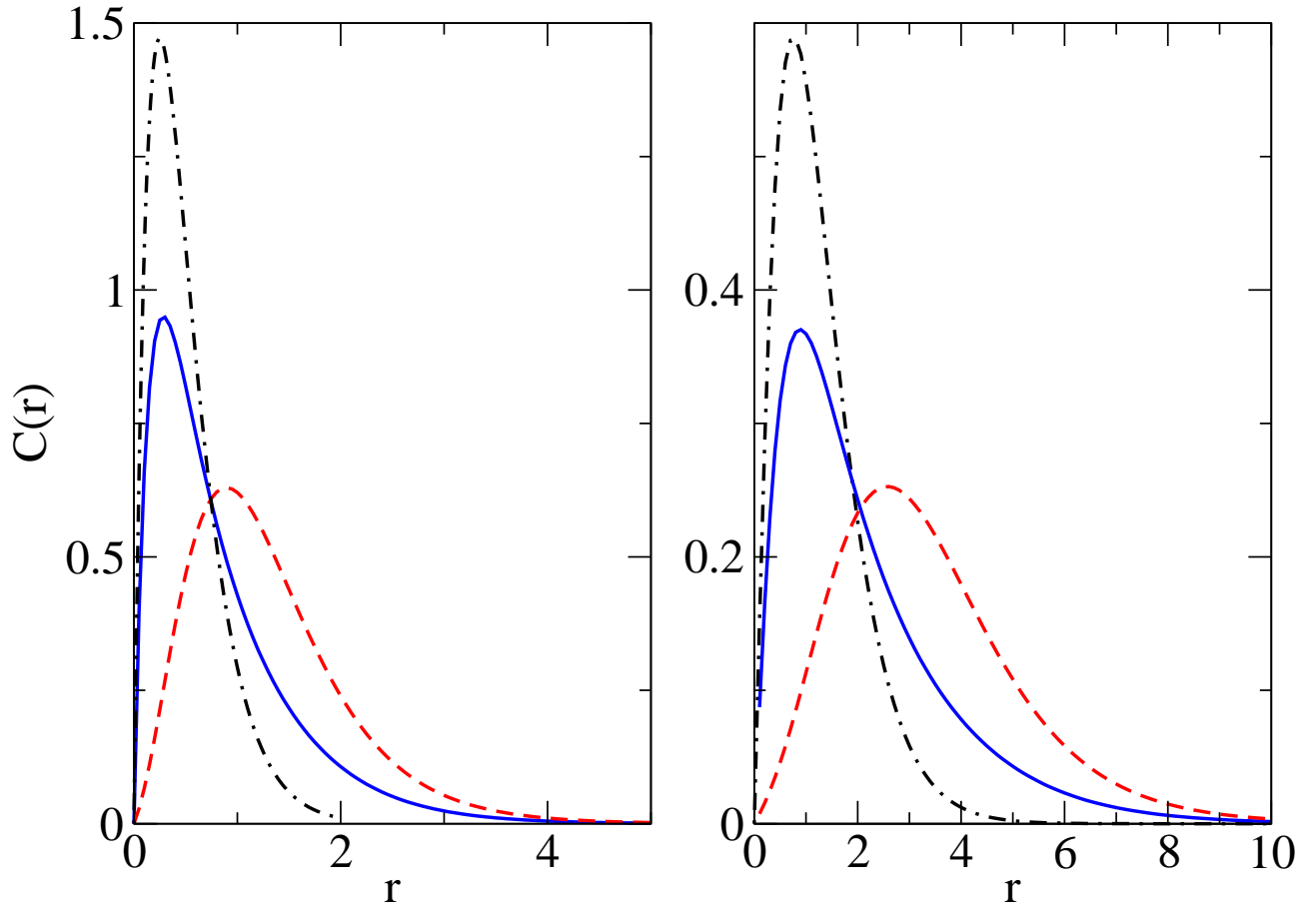


FIG. 4. Ground state correlation functions for  $\tilde{r}_0 = 0$  (left) and  $\tilde{r}_0 = 1$  (right). Electron-electron correlation,  $C_{ee}^t(r)$  (dashed line), electron-hole correlation,  $C_{eh}^t(r)$  (solid line), and exciton electron-hole correlation,  $C_{ee}^x(r)$  (dashed-dotted line).

- 13873 (2000).
- [49] Y. K. Ho, Phys. Rev. A **19**, 2347 (1979).
  - [50] J. Usukura and Y. Suzuki, Phys. Rev. A **66**, 010502 (2002).
  - [51] J. Z. Mezei, A. T. Kruppa, and K. Varga, Few-Body Systems **41**, 233 (2007).
  - [52] A. U. Hazi and H. S. Taylor, Phys. Rev. A **1**, 1109 (1970).
  - [53] Y. Ho, Physics Reports **99**, 1 (1983).
  - [54] N. Moiseyev, Physics Reports **302**, 212 (1998).
  - [55] Y. Suzuki and K. Varga, *Stochastic Variational Approach to Quantum-Mechanical Few-Body Problems* (Springer, 1998).
  - [56] J. Usukura, K. Varga, and Y. Suzuki, Phys. Rev. A **58**, 1918 (1998).
  - [57] L. V. Keldysh, JETP Lett. **29**, 658 (1979).
  - [58] D. Van Tuan, M. Yang, and H. Dery, Phys. Rev. B **98**, 125308 (2018).
  - [59] R. Krivec, V. B. Mandelzweig, and K. Varga, Phys. Rev. A **61**, 062503 (2000).
  - [60] J. Aguilar and J. M. Combes, Comm. Math. Phys. **22**, 269 (1971).
  - [61] E. Balslev and J. M. Combes, Comm. Math. Phys. **22**, 280 (1971).
  - [62] E. A. Hylleraas and B. Undheim, Zeitschrift für Physik **65**, 759 (1930).
  - [63] J. K. L. MacDonald, Phys. Rev. **43**, 830 (1933).
  - [64] F. M. Pont, P. Serra, and O. Osenda, Journal of Physics B: Atomic, Molecular and Optical Physics **44**, 135003 (2011).
  - [65] Y. Sajeev, Chemical Physics Letters **587**, 105 (2013).
  - [66] T. C. Thompson and D. G. Truhlar, Chemical Physics Letters **92**, 71 (1982).
  - [67] A. Macas and A. Riera, Chemical Physics Letters **164**, 359 (1989).
  - [68] P.-O. Lwidin, International Journal of Quantum Chemistry **27**, 495 (1985), <https://onlinelibrary.wiley.com/doi/pdf/10.1002/qua.560270414>.
  - [69] X. L. Yang, S. H. Guo, F. T. Chan, K. W. Wong, and W. Y. Ching, Phys. Rev. A **43**, 1186 (1991).
  - [70] T. P. Lyons, S. Dufferwiel, M. Brooks, F. Withers, T. Taniguchi, K. Watanabe, K. S. Novoselov, G. Burkard, and A. I. Tartakovskii, Nature Communications **10**, 2330 (2019).
  - [71] E. Liu, J. van Baren, Z. Lu, M. M. Altairy, T. Taniguchi, K. Watanabe, D. Smirnov, and C. H. Lui, Phys. Rev. Lett. **123**, 027401 (2019).
  - [72] A. M. Jones, H. Yu, J. R. Schaibley, J. Yan, D. G. Mandrus, T. Taniguchi, K. Watanabe, H. Dery, W. Yao, and X. Xu, Nature Physics **12**, 323 (2016).
  - [73] J. G. Roch, G. Froehlicher, N. Leisgang, P. Makk, K. Watanabe, T. Taniguchi, and R. J. Warburton, Nature Nanotechnology **14**, 432 (2019).

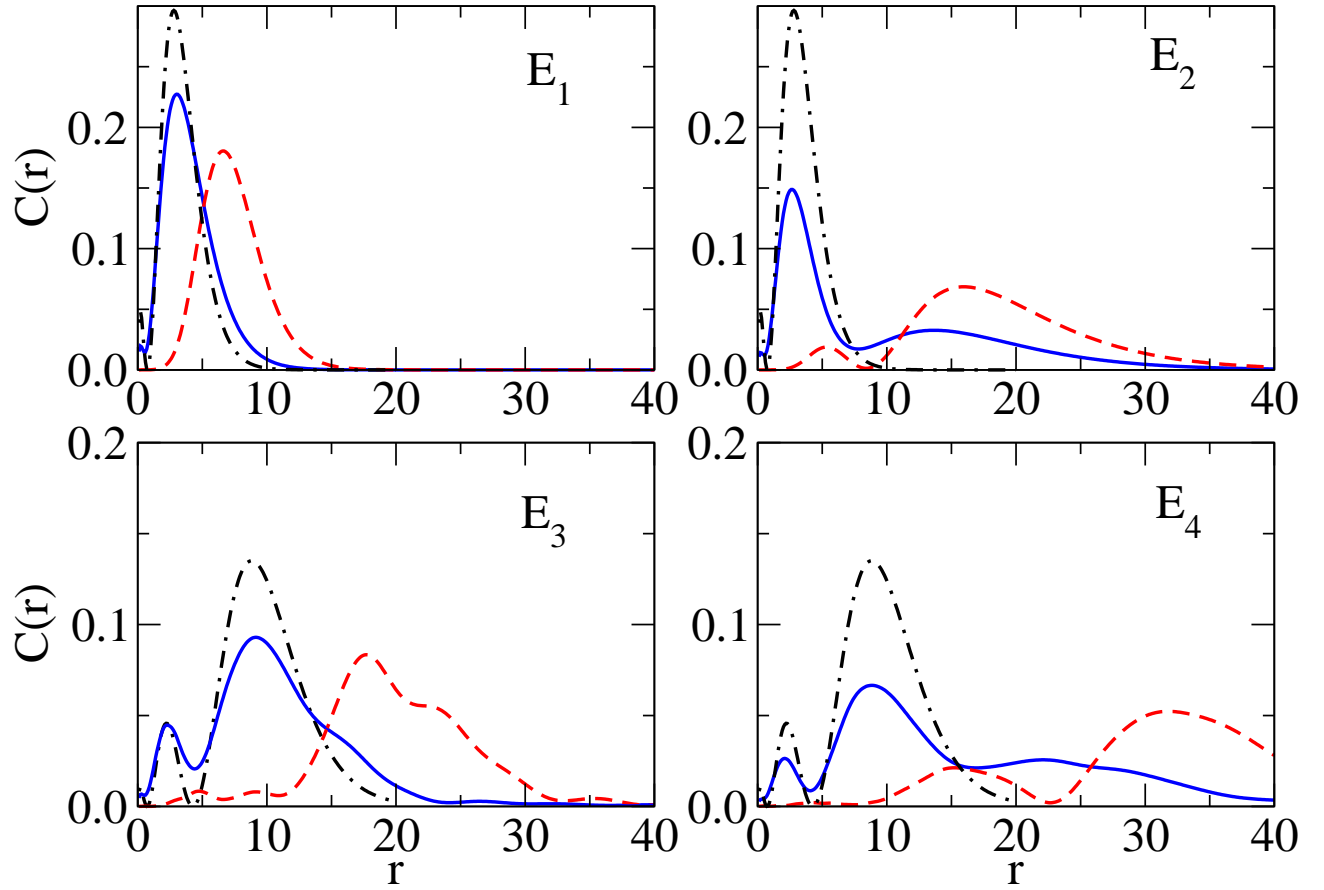


FIG. 5. Excited state correlation functions for  $\tilde{r}_0 = 0$ . Electron-electron correlation,  $C_{ee}^t(r)$  (dashed line), electron-hole correlation,  $C_{eh}^t(r)$  (solid line), and exciton electron-hole correlation,  $C_{ee}^x(r)$  (dashed-dotted line).

- [74] M. Goryca, J. Li, A. V. Stier, T. Taniguchi, K. Watanabe, E. Courtade, S. Shree, C. Robert, B. Urbaszek, X. Marie, and S. A. Crooker, *Nature Communications* **10**, 4172 (2019).
- [75] Mak Kin Fai, He Keliang, Lee Changgu, Lee Gwan Hyoung, Hone James, Heinz Tony F., and Shan Jie, *Nat. Mater.* **12**, 207211 (2013).
- [76] C. Robert, M. A. Semina, F. Cadiz, M. Manca, E. Courtade, T. Taniguchi, K. Watanabe, H. Cai, S. Tongay, B. Lassagne, P. Renucci, T. Amand, X. Marie, M. M. Glazov, and B. Urbaszek, *Phys. Rev. Materials* **2**, 011001 (2018).
- [77] B. Han, C. Robert, E. Courtade, M. Manca, S. Shree, T. Amand, P. Renucci, T. Taniguchi, K. Watanabe, X. Marie, L. E. Golub, M. M. Glazov, and B. Urbaszek, *Phys. Rev. X* **8**, 031073 (2018).
- [78] S.-Y. Chen, Z. Lu, T. Goldstein, J. Tong, A. Chaves, J. Kunstmann, L. S. R. Cavalcante, T. Woniak, G. Seifert, D. R. Reichman, T. Taniguchi, K. Watanabe, D. Smirnov, and J. Yan, *Nano Letters* **19**, 2464 (2019), PMID: 30860854.

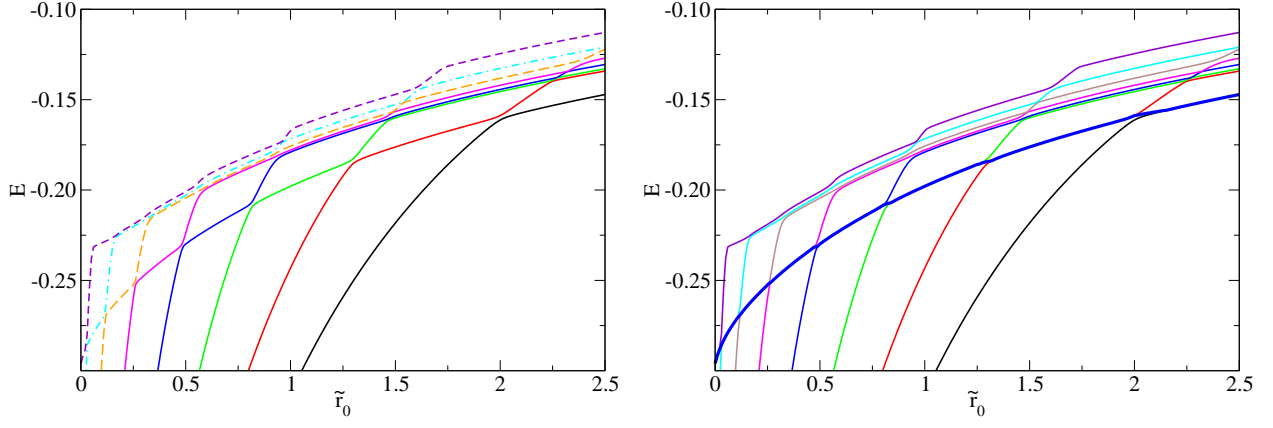


FIG. 6. Change of energy levels as a function of  $\tilde{r}_0$ . Left: By increasing  $\tilde{r}_0$  the potential weakens and the energy levels move upward. The energy of  $E_1$  moves upward but at around  $\tilde{r}_0=0.02$  the energy of the state below  $E_1$  moves up faster (dot dashed line) becomes nearly equal the energy of  $E_1$ . The two energy level cannot cross each other (avoided crossing) and  $E_1$  continues on the dot dashed line. The same thing happens at  $\tilde{r}_0=0.12$ , and  $E_1$  continues on the long dashed line, and so on. The path of  $E_1$  as a function of  $\tilde{r}_0$  is shown in the right (thick line).

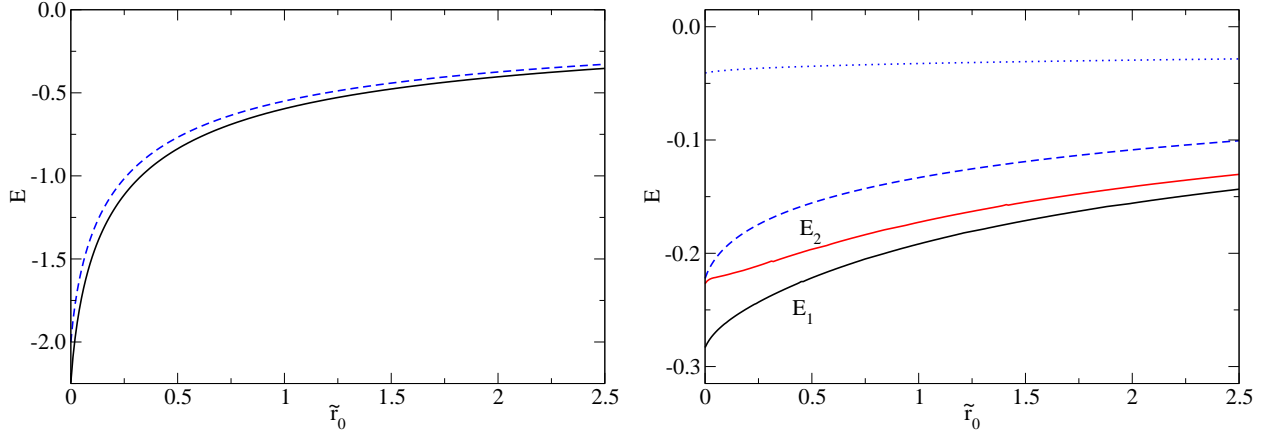


FIG. 7. Energies as a function of  $\tilde{r}_0$ . Ground state energy trion (solid line), 1s exciton energy (dashed line) (left); Excited state energies of trion (solid line), 2s exciton energy (dashed line), 3s exciton energy (dotted line) (right).



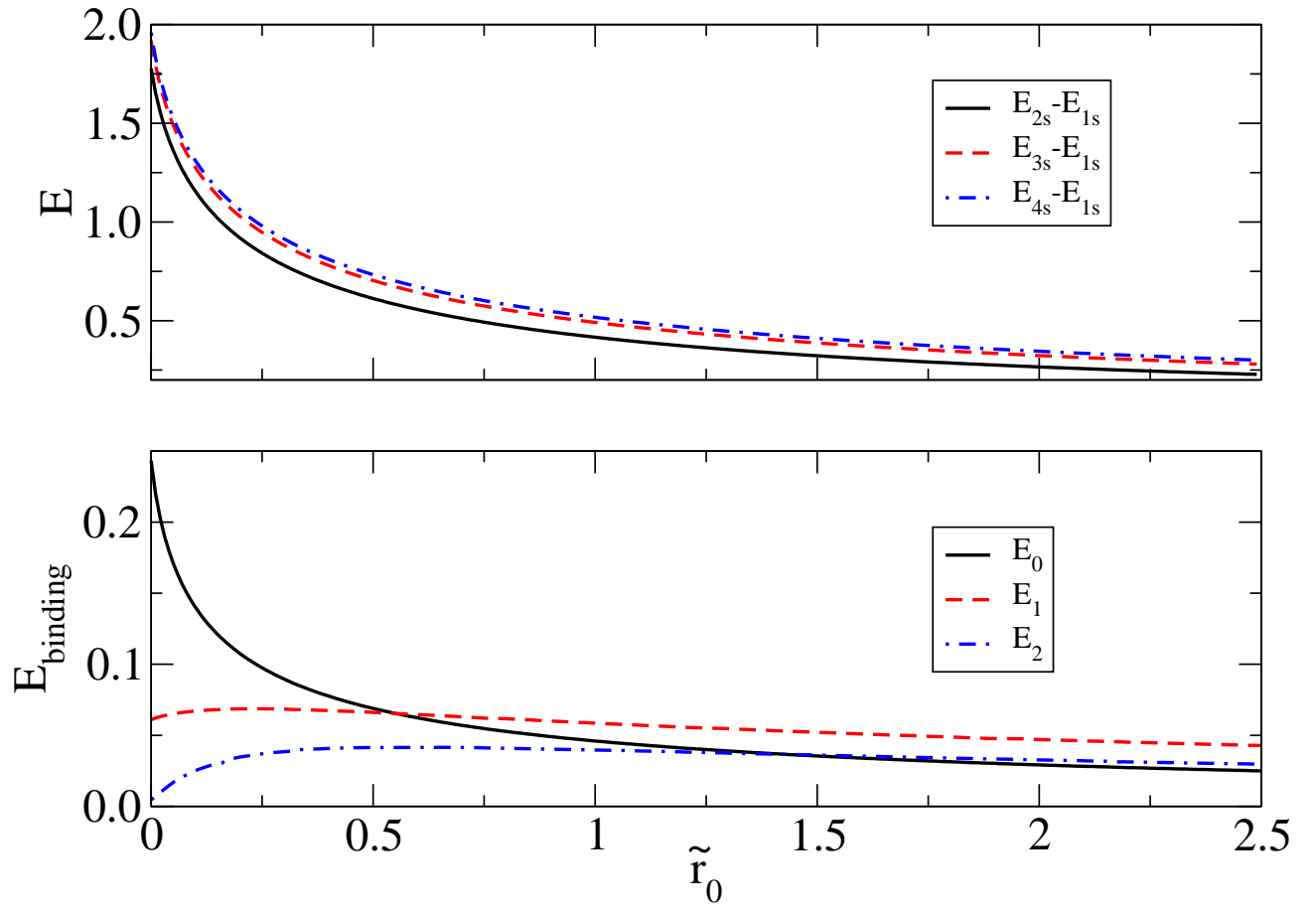


FIG. 8. Top: Transition energies of exciton excited states as a function of  $\tilde{r}_0$ . Bottom: Binding energies of the ground and the two lowest resonance states as a function of  $\tilde{r}_0$ .

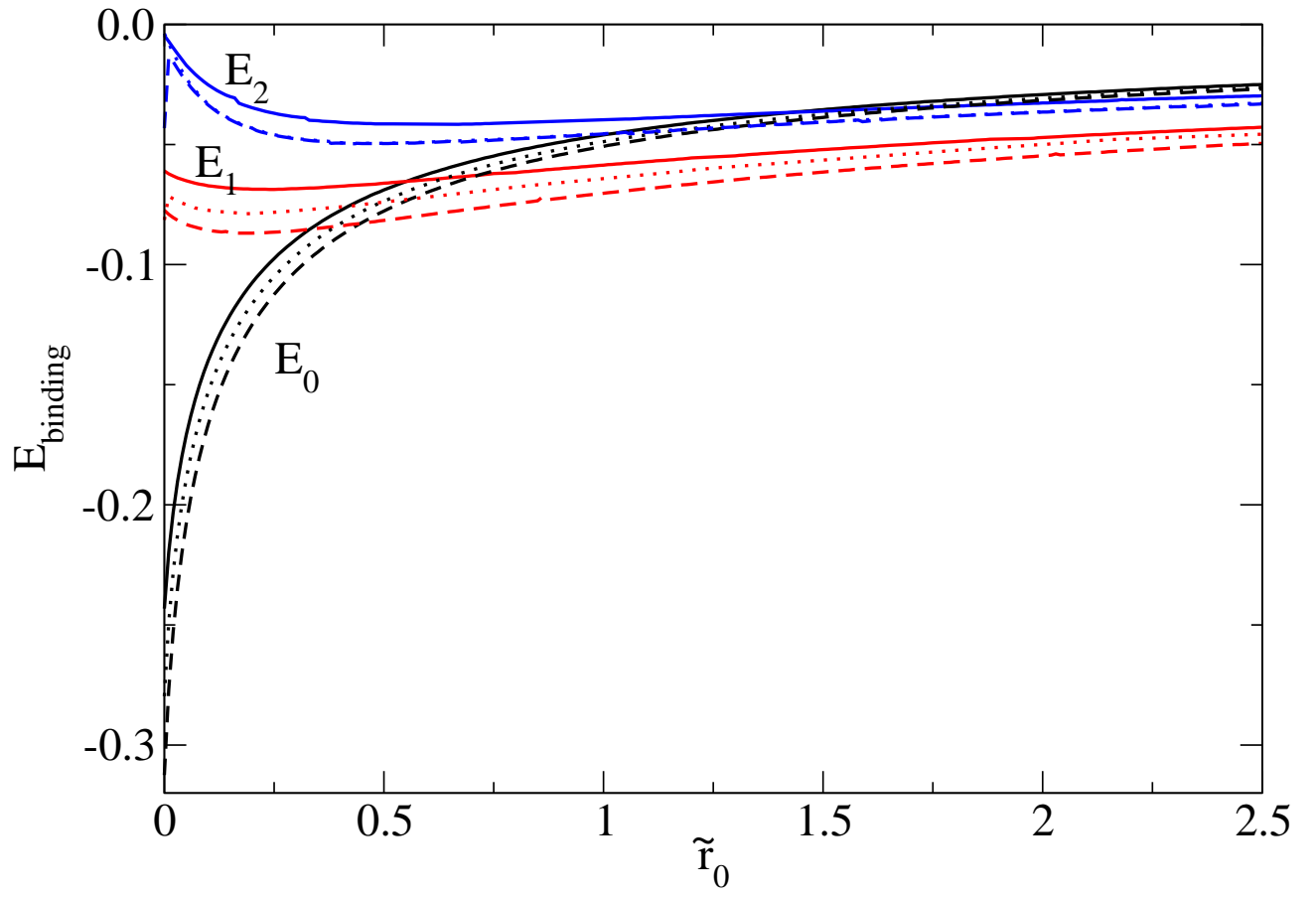


FIG. 9. Binding energies as a function of  $\tilde{r}_0$  (solid line  $eeh$  with  $\sigma = 1$ , dotted line  $eeh$  with  $\sigma = 2/3$ , dashed line  $ehh$  with  $\sigma = 2/3$ ).

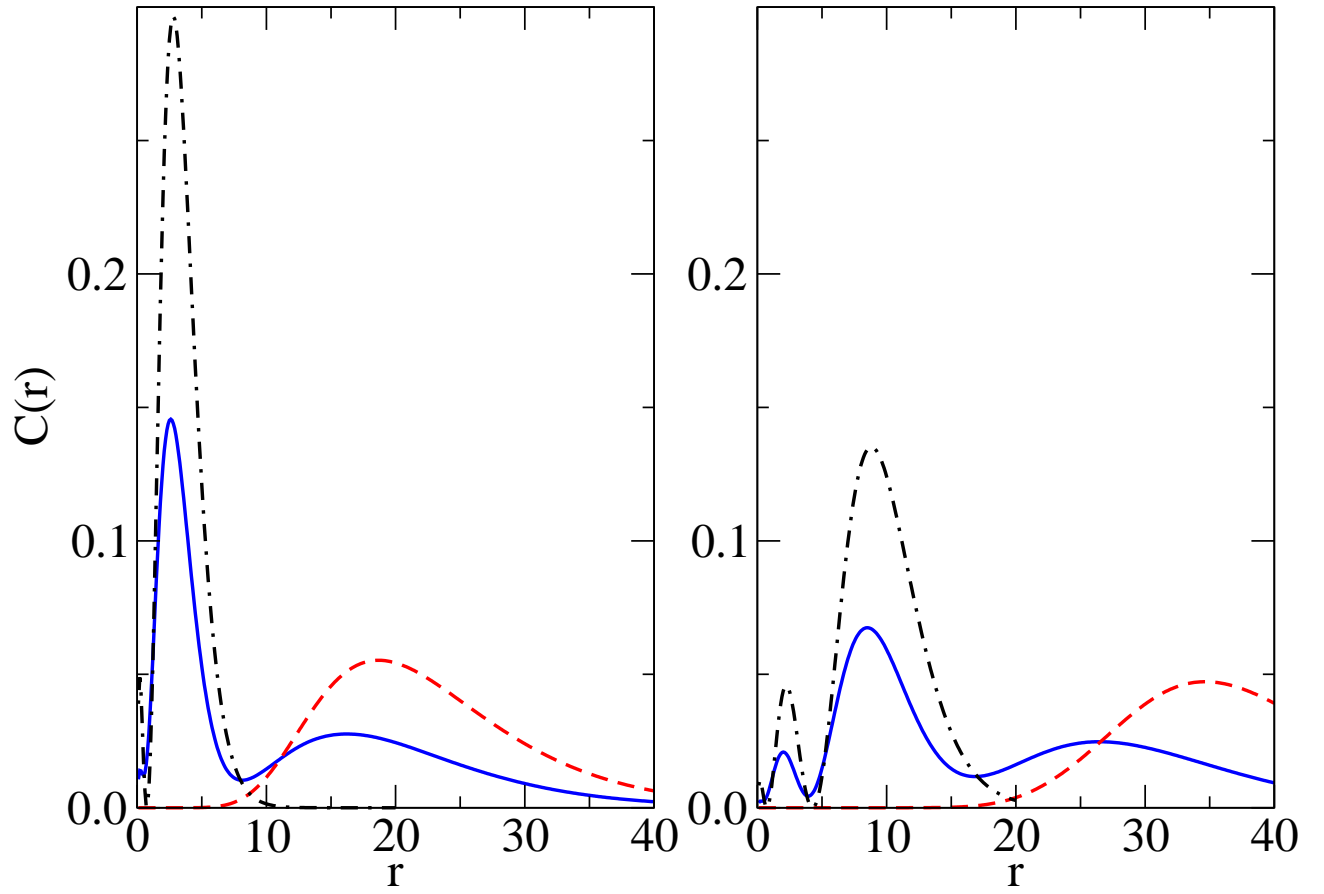


FIG. 10. Ground state correlation functions for  $S = 1$  resonances below the  $2s$  threshold (left) and below the  $3s$  threshold (right). Electron-electron correlation,  $C_{ee}^t(r)$  (dashed line), electron-hole correlation,  $C_{eh}^t(r)$  (solid line), and exciton electron-hole correlation,  $C_{ee}^x(r)$  (dashed-dotted line for  $2s$  exciton (left) and  $3s$  exciton (right)).